Journal of Directed Energy, 1, Fall 2005, 261–274

Investigation of Ultrafast Laser Ablation Using a Semiclassical Two-Temperature Model

J. K. Chen* and J. E. Beraun

Laser Effects Research Branch, Directed Energy Directorate, Air Force Research Laboratory, Kirtland Air Force Base, New Mexico 87117

and

D. Y. Tzou

Department of Mechanical and Aerospace Engineering, University of Missouri–Columbia, Columbia, Missouri 65211

A semiclassical two-temperature model is formulated, based on the Boltzmann transport equation, to solve thermal response of metals irradiated by an ultrashort-pulsed laser. In the simulation of laser material ablation, two competing mechanisms are considered: shock wave and phase explosion. Numerical analysis is performed for copper and gold films, respectively. It is shown that the present approach correlates well with experimental data over a wide range of laser fluences and pulse durations. It is also found that ultrashort-pulsed laser ablation could be caused by the generated shock wave for pulses of a few picoseconds or shorter and by the thermally induced phase explosion for the longer pulses.

KEYWORDS: Boltzmann transport equation, Hot-electron pressure, Phase explosion, Semiclassical two-temperature model, Shock wave, Ultrashort-pulsed laser ablation

Nomenclature

A_e, B_l	constant
b	ballistic range
C	heat capacity
C_{eo}	electron heat capacity constant
$\vec{E}$	electric field
e	charge of an electron
f	distribution function of electrons
G	electron–phonon coupling factor
G_{rt}	G at room temperature
H_m	fusion latent heat

Received February 4, 2004; revision received August 16, 2005.

*Corresponding author; current address: Department of Mechanical and Aerospace Engineering, University of Missouri–Columbia, Columbia, MO 65211; email: chenjnk@missouri.edu.

$\tilde{I}$	unit dyad
K	thermal conductivity
k_B	Boltzmann constant
m	mass of an electron
N	number density of atoms
n	number density of electrons
$\check{P}$	electron kinetic pressure dyad
p	isotropic electron kinetic pressure
p_{ij}	electron kinetic pressure components
$\bar{Q}_e$	electron heat flux vector
Q_x	heat flux in the x direction
q	number of total grid points
R	surface reflectivity
$\bar{r}$	position vector (x_i)
S	volumetric laser heat source
T	temperature
T_F	Fermi temperature
T_m	melting temperature
T_o	initial temperature
T_{tc}	thermodynamic equilibrium critical temperature
t	time
t_b	time of electron ballistic motion
t_{ml}	time when solid-to-liquid phase transformation is complete
t_{ms}	time when solid-to-liquid phase transformation starts
t_p	pulse duration defined as full width at half-maximum
U_o	bond energy of atom
$\bar{u}$	group velocity vector (u_i)
V_F	Fermi velocity
V_s	speed of sound
v_x	drift velocity in the x direction
$\bar{v}$	mean (drift) velocity vector
W	electron energy, $(\Gamma + nm\lvert\bar{v}\rvert^2)/2$
w	electron energy density
X	film thickness
x, y, z	spatial coordinates
α	optical penetration depth
β	$10^{-8} \times T_e$ [V/K]
$\chi, \gamma, \eta, \kappa$	constant
δ	ablation depth
ϕ	laser fluence
$\phi_{\mathrm{th}}^{\alpha}, \phi_{\mathrm{th}}^{\hat{\lambda}}$	ablation threshold for low and high laser fluence, respectively
Γ	$p_{xx} + p_{yy} + p_{zz}$
λ	effective electron heat diffusion length
θ_e	dimensionless electron temperature, T_e/T_F
θ_l	dimensionless lattice temperature, T_l/T_F
ρ	lattice mass density
τ	relaxation time

τ_{e-p} energy relaxation time
τ_k momentum relaxation time

1. Introduction

Studies of ultrashort-pulsed laser-material interaction have become one of the main topics of research in the past decade.[2,4,6,8,9,11,13,15,17,18,20,22,24,25] Numerous theoretical models are proposed for predicting the amount of material ablated by ultrashort-pulsed lasers; however, none of them has demonstrated the capability of accurately capturing the ablation response over a wide range of laser fluences and pulse durations. The main reasons are as follows: 1) the models may not be comprehensive due to the fact that a complete understanding of the physics involved in the process is still missing and 2) the material properties used in the simulations are not well characterized and quantified.

With the assumptions that the heat capacities of free electrons and the lattice, as well as the thermal conductivity of electrons, are temperature independent and with the conditions that $\alpha \gg$ or $\ll \lambda$, Nolte et al.[18] deduced two logarithmic functions for the dependence of ablation depth: $\delta = \alpha \ln(\phi/\phi_{\text{th}}^{\alpha})$ for low laser fluences and $\delta = \lambda \ln(\phi/\phi_{\text{th}}^{\lambda})$ for high fluences. Comparison with their experimental data showed that the logarithmic dependence exists for pulses shorter than 20 ps, whereas the two constants α and λ and the ablation thresholds $\phi_{\text{th}}^{\alpha}$ and $\phi_{\text{th}}^{\lambda}$ vary with pulse length, especially for the longer pulses. By relaxing the extreme conditions $\alpha \gg$ and $\ll \lambda$, Vatsya and Virk[22] obtained an approximate solution of the ablation depth for a wide range of laser fluence. Although a more complete description of the process is necessary, it appears that the above approximations provided an insight into the qualitative behavior of the results. On the basis of the force that the electric field of charge separation pulls the ions out of a target, Gamaly et al.[9] derived two analytical formulas for the ablation threshold and depth for laser pulses in the range of 10^{13}–10^{14} W/cm^2. In the numerical simulation, Komashko et al.[13] implemented a vector optical propagation scheme that accounts for laser polarization and the angle of incidence into a one-dimensional (1D) radiation-hydrodynamic code for ultrashort laser pulse interaction with aluminum (since a reliable equation of state suited for the laser ablation regime is available for aluminum). By taking into account the hydrodynamic plasma expansion, degeneracy of the electron gas, cold pressure of ions, and interaction between the electron and ion subsystems, as well as assuming that laser ablation occurs when ion temperature is close to a critical value 0.1–$0.2U_o$, Zavestovskaya et al.[25] developed another numerical model for the ultrashort laser material ablation. The simulated amount of material ablated by a 150-fs laser pulse was in good agreement with the experimental data.[18] A simpler approach using the thermal analysis along with a phase explosion mechanism was considered by numerous researchers.[4,6,24] In this approach, laser ablation was assumed to take place when the temperature of a metastable (superheated) liquid reaches the point near the thermodynamic equilibrium critical temperature.[11] In contrast to the above thermal ablation mechanisms,[4,6,18,22,24,25] Afanasiev et al.[2] asserted a nonthermal mechanism that the material behind a pressure front that is greater than the characteristic pressure in a solid would be removed in a gas phase. In an attempt to identify the ultrafast ablation mechanisms, Zhigilei and his associates[15,20] conducted a series of studies on the photomechanical spallation using molecular dynamics. They found that the relaxation of laser-induced thermoelastic stresses is responsible for the nucleation, growth, and coalescence of voids in a broad subsurface region of the irradiated target. A similar study was reported by Cheng and Xu.[8]

In the aforementioned theoretical investigations, the temperature fields in electrons and the lattice are solved with the framework of the phenomenological two-temperature (2T) models.[3,5] In a nonuniformly heated conductor in the absence of current, there arises an electric field.[1] If the electric field and the carrier gradient become excessively large, then nonequilibrium transport conditions will occur.[21] This is particularly true for ultrashort laser heating due to the fact that a tremendously sharp gradient of the electron temperature (or free electron density) is present in a small geometry encountered. In such a case, the widely used, phenomenological 2T models may not be able to accurately capture the thermal response of electrons and the lattice. To establish more adequate equations for the nonequilibrium electron effects, there is a need to examine the transport equations based on the Boltzmann approximation.

In this paper, a semiclassical 2T model is formulated to investigate thermal transport in metal solids subjected to ultrashort laser heating. With the first three moments of the Boltzmann transport equation, the equations that govern the conservation of number density, momentum, and energy are derived for the electron subsystem. Temperature fields in the electrons and the lattice are solved with the equations of the conservation of momentum and energy in the electrons and the equation of heat conduction in the lattice. In the simulation of material ablation, two competing mechanisms are considered: shock wave (nonthermal)[2] and phase explosion (thermal).[11] Numerical analyses are performed for copper and gold films. The results are compared with the experimental data in the open literature.

2. Semiclassical Two-Temperature Model

The phenomenological, dual-hyperbolic 2T model proposed by Chen and Beraun[6] for ultrashort-pulsed laser material ablations is given as follows:

$$C_e\frac{\partial T_e}{\partial t}+\frac{\partial Q_{ex}}{\partial x}=-G\,(T_e-T_l)+S(x,t), \tag{1}$$

$$\tau_e\frac{\partial Q_{ex}}{\partial t}+Q_{ex}=-K_e\frac{\partial T_e}{\partial x}, \tag{2}$$

$$C_l\frac{\partial T_l}{\partial t}=-\frac{\partial Q_{lx}}{\partial x}+G(T_e-T_l)\qquad (T_l\neq T_m), \tag{3}$$

$$\int_{t_{ms}}^{t_{ml}}\left[-\frac{\partial Q_{lx}}{\partial x}+G(T_e-T_l)\right]dt=\rho H_m\qquad (T_l=T_m), \tag{4}$$

$$\tau_l\frac{\partial Q_{lx}}{\partial t}+Q_{lx}=-K_l\frac{\partial T_l}{\partial x}. \tag{5}$$

In the above equations the quantities with subscripts e and l are associated with the electrons and the lattice, respectively. For pure metals, the heat flux in the lattice Q_{lx} and in Eq. (5) are often neglected since $K_e \gg K_l$. Equation (4) assumes that while melting, the lattice temperature remains unchanged until the solid-to-liquid phase transformation is complete. The start time (t_{ms}) of the phase change is determined from Eq. (3), and the end time (t_{ml}) by Eq. (4). Despite that the melting point of a superheated solid is somewhat higher than the normal point and that the solid-to-liquid phase transformation generally is nonisothermal, the above isothermal phase transformation assumption is tolerable for predicting the amount of ablated material.

Instead of using the energy balance equation (1) to solve the electron temperature, three semiclassical transport equations are formulated below to accommodate the electron

concentration, the mean (drift) velocity, and the average energy based on the Boltzmann transport approximation. Let $f(\bar{r}, \bar{u}, t)$ be a distribution function of electrons at time t in the phase space with position vector ($\bar{r}$) and velocity vector ($\bar{u}$). If the Lorentz force due to magnetic fields is neglected, the Boltzmann transport equation for electrons becomes

$$\frac{df}{dt} = \frac{\partial f}{\partial t} + \bar{u} \cdot \nabla_r f + \frac{e}{m} \bar{E} \cdot \nabla_u f = \left(\frac{\partial f}{\partial t} \right)_c , \tag{6}$$

where $\nabla_r = \partial / \partial x_i$ and $\nabla_u = \partial / \partial u_i$ (the index $i = 1, 2, 3$ refers to spatial coordinates x, y, and z, respectively); $e\bar{E}/m$ is the Lorentz force resulting from the electric field. The total derivative $\mathrm{d}f/\mathrm{d}t$ is evaluated along the trajectory $\bar{r} = \bar{r}(t)$ and $\bar{u} = \bar{u}(t)$ in the absence of collision. The term $(\partial f/\partial t)_c$ on the right-hand side of Eq. (6) is the time-rate of change of f due to collision.

Similar to the procedure in Ref. 14, the equations of the conservation of the number density, momentum, and energy for the electron gas are derived with the first three moments of the Boltzmann equation (6). For brevity, only the results are given here:

$$\frac{\partial n}{\partial t} + \nabla_r \cdot (n\bar{v}) = \left(\frac{\partial n}{\partial t} \right)_c , \tag{7}$$

$$m \frac{\partial \bar{v}}{\partial t} + m\bar{v} \cdot (\nabla_r \bar{v}) - e\bar{E} + \frac{1}{n} \nabla_r \cdot \tilde{P} = m \left(\frac{\partial \bar{v}}{\partial t} \right)_c , \tag{8}$$

$$\frac{\partial W}{\partial t} + \nabla_r \cdot \left(\frac{\Gamma}{2} \bar{v} + \bar{v} \cdot \tilde{P} \right) + \frac{m}{2} \nabla_r \cdot (n |\bar{v}|^2 \bar{v}) + \nabla_r \cdot \bar{Q}_e - ne\bar{E} \cdot \bar{v} = \left(\frac{\partial W}{\partial t} \right)_c , \tag{9}$$

where the kinetic pressure dyad $\tilde{P}$ is defined as $p_{ij} \bar{i}\bar{j}$ with $\bar{i}$ and $\bar{j}$ being the unit vectors and i, $j = x, y, z$, respectively. Under the assumption of an isotropic Maxwell–Boltzmann distribution of peculiar velocities, the electron kinetic pressure is isotropic, i.e., $\tilde{P} = p\tilde{I} = nk_B T_e \tilde{I}$. The electric field generated in a nonuniformly heated conductor in the absence of current is $\bar{E} = \beta \nabla T_e$, where $\beta \sim 10^{-8} T_e$ [V/K] for free electrons.[1] The collision term in Eq. (8) that represents the time rate of change of momentum density due to intraband collisions and generation-recombination processes is approximated by

$$m \left(\frac{\partial \bar{v}}{\partial t} \right)_c = -m \frac{\bar{v}}{\tau_k} \tag{10}$$

in which the momentum relaxation time is temperature dependent, $\tau_k = \gamma T_e^{-1}$, with γ being a constant.[16]

It is well-known that only those electrons in states within the energy range $k_B T$ can be excited thermally at temperature T. If one atom gives one valence electron to the free electron gas, the excited electrons can be determined for temperatures $T < 0.1 T_F$ (Ref. 12):

$$n = \tfrac{1}{3} \pi^2 N (T_e / T_F). \tag{11}$$

The renowned linear relationship of electron heat capacity is thus derived:

$$C_e = \tfrac{3}{2} n k_B = \tfrac{1}{2} \pi^2 N k_B (T_e / T_F) = C_{eo} T_e \tag{12}$$

with the constant $C_{eo} = \pi^2 N k_B / 2T_F$. By making use of Eq. (12), the electron kinetic pressure p is expressed as a function of T_e:

$$p = \tfrac{2}{3} C_{eo} T_e^2 . \tag{13}$$

Substitution of $\tilde{P} = p\tilde{I}$ with p given by Eq. (13) and the two relationships $\bar{E} = \beta \nabla T_e$ and $(\partial \bar{v}/\partial t)_c = \bar{v} T_e/\gamma$ into Eq. (8) results in

$$m\frac{\partial \bar{v}}{\partial t} + m\bar{v} \cdot (\nabla_r \bar{v}) + (2k_B - e\beta)\nabla T_e = -\frac{m\bar{v}T_e}{\gamma}. \tag{14}$$

This momentum equation clearly indicates that the electron drift velocity $\bar{v}$ is solely a function of the electron temperature.

Similarly, the energy equation (9) can be rewritten in the form

$$\frac{\partial w}{\partial t} + \bar{v} \cdot \nabla_r w + \frac{1}{n}\nabla_r \cdot (nk_B T_e \bar{v}) + \frac{1}{n}\nabla_r \cdot \bar{Q}_e - e\beta \bar{v} \cdot \nabla_r T_e = \left(\frac{\partial w}{\partial t}\right)_c, \tag{15}$$

where the electron energy density is defined as $w = m|\bar{v}|^2/2 + 3k_B T_e/2$. The collision term on the right-hand side of Eq. (15), $(\partial w/\partial t)_c$, represents the time rate of change of electron energy density due to the electron–phonon scattering and the generation–recombination and is approximated by $(\partial w/\partial t)_c = -(w - w_l)/\tau_{e-p}$, with w_l denoting the equilibrium energy when $T_e = T_l$ and τ_{e-p} being the energy relaxation time. Equation (15) can be further simplified by making use of the momentum equation (14):

$$C_e\left(\frac{\partial T_e}{\partial t} + \bar{v} \cdot \nabla_r T_e + \frac{2}{3}T_e \nabla_r \cdot \bar{v}\right) + \nabla_r \cdot \bar{Q}_e = C_e\left(\frac{\partial T_e}{\partial t}\right)_c. \tag{16}$$

The term $C_e(\partial T_e/\partial t)_c$ in Eq. (16) is approximated to be $C_e(T_e - T_l)/\tau_{e-p}$, which is the time rate of thermal energy exchange between the electrons and lattice. By including the optical-electron scattering due to laser excitation, the energy equation then becomes

$$C_e\left(\frac{\partial T_e}{\partial t} + \bar{v} \cdot \nabla_r T_e + \frac{2}{3}T_e \nabla_r \cdot \bar{v}\right) + \nabla_r \cdot \bar{Q}_e = -G(T_e - T_l) + S(\bar{r}, t), \tag{17}$$

where the electron–phonon coupling factor $G = C_e/\tau_{e-p}$.

The semiclassical 2T model obtained above governs the ultrafast thermal transport in metal solids. It includes the equations of the conservation of momentum and energy in the electron subsystem, (14) and (17); the energy balance equation for the lattice subsystem, (3); the equation for the solid-to-liquid phase transformation, (4); and the constitutive equations for the heat fluxes, (2) and (5). The difference between the semiclassical and phenomenological 2T models is that the former includes the effects of the electron drifting, resulting from the generated electric field and the electron kinetic pressure. For a 1D transport problem, for instance, five equations are to be satisfied by the five unknowns Q_{ex}, T_e, v_x, Q_{lx}, and T_l. On the other hand, the phenomenological dual-hyperbolic 2T models involve four unknowns, Q_{ex}, T_e, Q_{lx}, and T_l, to be solved. Like the phenomenological models, the semiclassical 2T model can be simplified with the assumptions $\bar{Q}_l$ and/or $\tau_e = 0$.

3. Solution Algorithm

A 1D problem of metal materials ablated by ultrashort-pulsed lasers is analyzed in this paper since the laser spot sizes are much larger than the depth of the thermally affected zone for the time period of interest. The 1D version of the governing equations (2), (3)–(5) with $Q_{lx} = 0$, (14), and (17), together with the following initial and boundary conditions, are solved with a central difference method[6]:

$$T_e(x, 0) = T_l(x, 0) = T_o; \qquad v_x(x, 0) = 0, \tag{18}$$

$$Q_{ex}(0, t) = Q_{ex}(X, t) = 0, \tag{19}$$

where T_o is set to be 300 K and X is the current thickness of the material.

As material is ablated in a plasma, vapor, and/or liquid phase,[17] the shielding (absorption) of laser radiation by the removed material may play a significant role in the laser energy deposition into the material. For simplicity, attenuation of the volumetric laser heat source by the ejected plasma, vapor, and/or liquid is simply assumed to be proportional to the ablation depth. Thus, the 1D laser heat source is expressed as

$$S(x,t) = \sqrt{\frac{4\ln 2}{\pi}}\frac{(1-R)\phi}{\alpha t_p}\exp\left\{-\left(\frac{\kappa\delta(t)+X(t)-x}{\alpha}\right)-4\ln 2\left[\left(\frac{t-2t_p}{t_p}\right)^2\right]\right\}, \tag{20}$$

where κ is a constant. Lasing is assumed to start at $t=0$ and end at $t=4t_p$. The laser energy outside this period of time is neglected in this work since it is too small to significantly alter the result. When $\delta > 0$, the laser intensity at the surface of the material, $x = X(t)$, is reduced by a factor of $\exp[-(\kappa\delta)/\alpha]$. The laser heat source distribution over the thickness thus becomes $\exp[-(\kappa\delta + X - x)/\alpha]$. It should be noted here that an intrinsic assumption that the excited electrons are immediately and fully thermalized is made when Eq. (20) is directly applied to a 2T model.

Immediately after a metal solid is illuminated by an ultrashort-pulsed laser, while the excited electrons are still highly nonequilibrium, two competing processes take place. The nonthermalized electrons move ballistically with a velocity close to the Fermi velocity. Through collision, meanwhile, those nonthermalized electrons continue to thermalize into a Fermi–Dirac distribution in which the electron temperature can be measured. It takes some time for the excited electrons to complete the ballistic motion and the thermalization process. Therefore, the heat source given by Eq. (20) needs to be modified should the two effects on the thermal response become crucial. Since the laser fluences considered in this paper are very high (beyond the ablation threshold), the effects of electron thermalization on the laser heat source are neglected for simplicity.

To account for the electron ballistic transport, an effective absorption depth that includes the optical penetration depth and the ballistic range (b) is introduced.[10,23] For instance, a ballistic range of 105 nm is assumed for gold based on the postulation that nonequilibrium electrons penetrate into the nonexcited region for about 100 fs. With this approach the spatial function in Eq. (20) is replaced with $\exp[-(\kappa\delta + X - x)/(\alpha + b)]$. Instead of imposing a ballistic range on the optical penetration depth, we assume that the nonthermal equilibrium electrons scatter at an isotropic (random) Fermi velocity for a finite period of time (t_b). Upon the excitation by a laser pulse, the spatial distribution of the laser heat source is described by Eq. (20). The heat source then attenuates as the nonthermalized electrons propagate. For a grid spacing of Δx, it takes a finite time interval $\Delta t = \Delta x / V_F$ for those electrons to move from a grid point to its neighbor points. Hence, the spatial distribution of the heat source after each time interval becomes $S_i = (S_{i-1} + S_{i+1})/2$ for the interior grid points ($i = 2, \ldots, q-1$) and $S_1 = (S_1 + S_2)/2$ and $S_q = (S_{q-1} + S_q)/2$ for the boundary points, where $S_i = S(x_i, t)$ for these terms on the left-hand sides and $S_i = S(x_i, t - \Delta t)$ for those on the right-hand sides. Redistribution of the heat source continues for $\mathcal{N}$ times, where $\mathcal{N}$ is determined by the relationship $\mathcal{N}\Delta x / V_F = t_b$.

Two competing ablation mechanisms are considered here: shock wave and phase explosion. The latter assumes that a laser ablation occurs when the temperature of a metastable (superheated) liquid is equal to or greater than $0.9T_{tc}$ (Refs. 6 and 11). Under this criterion, the liquid whose lattice temperature meets the above condition will be removed from the bulk. On the other hand, the former assumes that a laser ablation takes place when the peak pressure generated in a solid is higher than the characteristic pressure ρV_s^2 of the material.[2]

Since the characteristic diffusion velocity of electron thermal energy, $(K_e/C_e\tau_e)^{1/2}$, is much faster than the speed of sound, the lattice motion is essentially initiated by the electron kinetic pressure ($p = 2C_{eo}T_e^2/3$). Under this assumption, the material behind the peak electron kinetic pressure that is greater than ρV_s^2 will be removed from the bulk. In the numerical simulation, the type of abaltion is determined by which condition, the electron kinetic pressure or the lattice temperature, is first met. The grid point(s) that undergo ablation are eliminated from the model. In case the ablation occurs at a point underneath the irradiated surface, all the grid points that locate from the irradiated surface to the point are removed.

4. Numerical Results

The numerical analysis is performed for copper and gold films. The material parameters of the two materials used in the simulations are given in Table 1, Fig. 1, and the equations below, unless otherwise mentioned. The thermal conductivity and the relaxation time of electrons and the electron–phonon coupling factor are expressed in the forms[7]

$$K_e = \chi \frac{(\theta_e^2 + 0.16)^{\frac{5}{4}}(\theta_e^2 + 0.44)\theta_e}{(\theta_e^2 + 0.092)^{\frac{1}{2}}(\theta_e^2 + \eta\theta_l)}, \tag{21}$$

$$\tau_e(T_e, T_l) = \frac{1}{A_e T_e^2 + B_l T_l}, \tag{22}$$

$$G = G_{RT}\left[\frac{A_e}{B_l}(T_e + T_l) + 1\right]. \tag{23}$$

Table 1. Material parameters used in the simulations

Parameter	Copper	Gold
ρ, kg/m^3	8.93×10^3	1.93×10^4
C_{eo}, Jm^{-3}K^{-2}	96.6	70
H_m, Jkg^{-1}	2.068×10^5	6.275×10^4
χ, Wm^{-1}K^{-1}	377	353
η	0.139	0.16
R	0.65	0.58
α, nm	14.0	14.5
A_e, K^{-2}s^{-1}	1.75×10^7	1.2×10^7
B_l, K^{-1}s^{-1}	1.98×10^{11}	1.23×10^{11}
G_{RT}, Wm^{-3}K^{-1}	1.0×10^{17}	2.2×10^{16}
T_m, K	1,357	1,337
T_{ic}, K	5,760	7,670
T_F, K	8.12×10^4	6.4×10^4
p_o, Gpa	202.2	189.9
β, V/K	10^{-8}	10^{-8}
t_b, fs	100	100
γ, sK	0.333×10^{-15}	0.333×10^{-15}

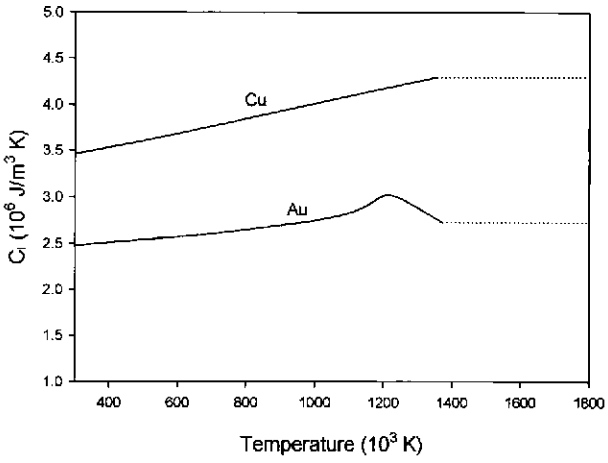

Fig. 1. Heat capacities of copper and gold lattices.

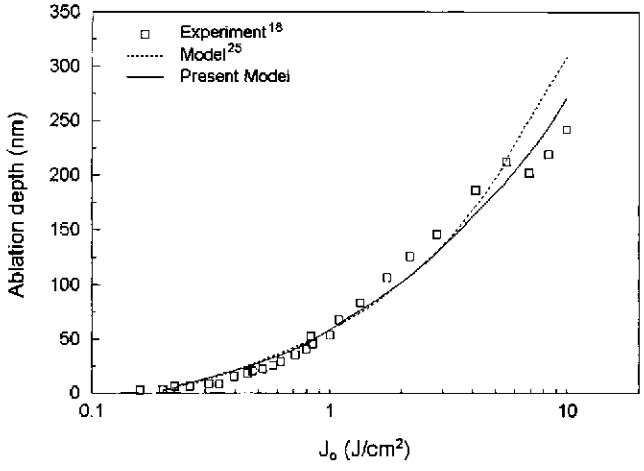

Fig. 2. Comparison of the simulated ablation depth with experimental data for copper heated by a 150-fs laser pulse ($\kappa = 0$).

Figure 1 gives the temperature-dependent heat capacities, where the lattice heat capacity C_l is calculated from the relationship $C = C_e + C_l$ for $T_l \leq T_m$, with C being the bulk heat capacity and assumed to be constant for $T_l \geq T_m$. A finite difference model composed of equally spaced grid points is employed to solve temperature in the electron and lattice subsystems. Resolution of the model and the time increment is first studied with three different sizes of grid space: 0.5, 1.0, and 2.0 nm. It is found that a grid size of 1 nm is adequate to resolve the problem. Therefore, the uniform-mesh models of 1-nm grid size are employed in the following calculations. The time increments used are $(2.0–5.0) \times 10^{-18}$ s (depending on the laser pulse length) for copper and 2.5×10^{-17} s for gold.

Figure 2 compares the calculated ablation depth with the experimental data[18] for copper heated by a 150-fs laser pulse with fluences up to 10 J/cm^2. The value of κ used in this

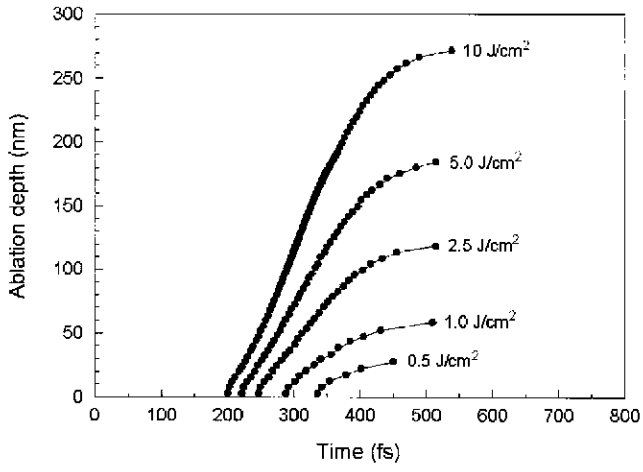

Fig. 3. Material ablation process simulated for copper heated by a 150-fs laser pulse.

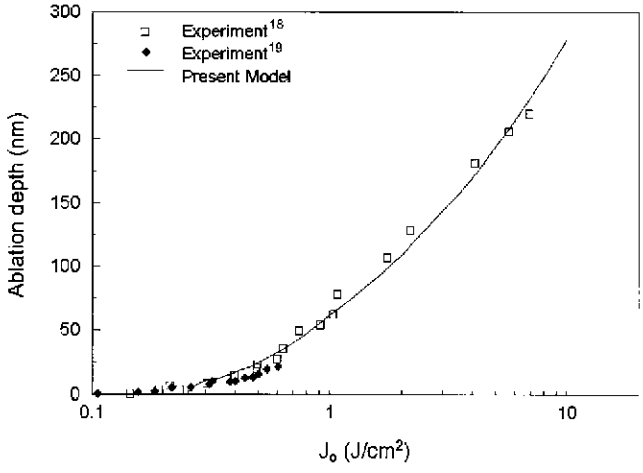

Fig. 4. Comparison of the simulated ablation depth with experimental data for copper heated by a 500-fs laser pulse ($\kappa = 0.08$).

simulation is zero. For comparison, the result obtained from a more complex model[25] is also presented. It appears that both models correlate fairly well with the experimental data, including the ablation threshold. The difference between the two models is inconsequential until the fluence is greater than 4 J/cm^2. Figure 3 shows the simulated time history of material removal for five different fluences. It is found that the material ablation by this 150-fs pulse is caused by the generated shock wave and takes place somewhere underneath the heated surface except for the 10-J/cm^2 case, in which a portion of the material, from the depth $x = 96$ to 193 nm, is ablated from the surface. The sizes of the material ablated each time are from one to several nanometers. The calculated phonon temperature of the ablated material when it is removed is around 500 K.

Figures 4–6 compare the calculated ablation depth and the experimental data[18,19] for three longer laser pulses, 500 fs, 2 ps, and 14.4 ps, respectively. For these cases, the values

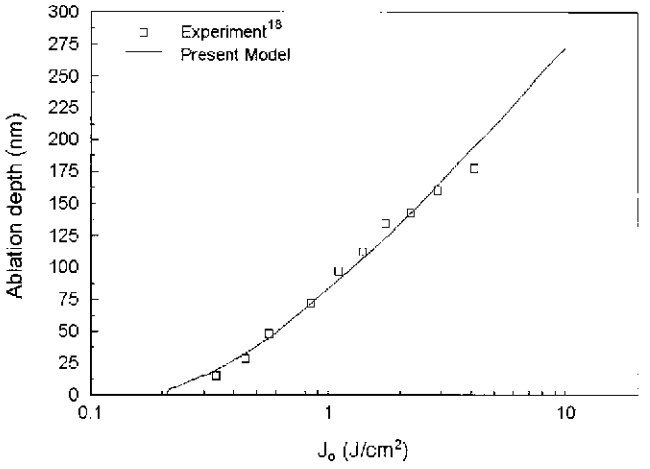

Fig. 5. Comparison of the simulated ablation depth with experimental data for copper heated by a 2-ps laser pulse ($R = 0.3$, $\kappa = 0.15$).

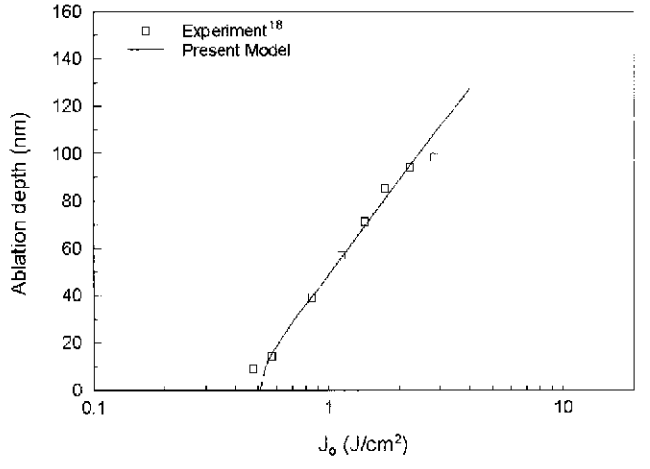

Fig. 6. Comparison of the simulated ablation depth with experimental data for copper heated by a 14.4-ps laser pulse ($R = 0.58$, $\kappa = 0.2$).

of R and κ employed are 0.65 and 0.08, 0.3 and 0.15, and 0.58 and 0.2, respectively. This fact reveals that the shielding of laser radiation by the ejected plasma, vapor, and/or liquid does influence the laser energy deposition into the material and, in turn, the ablation result. Again, the present results show good agreement with the experimental data. The ablations found from these simulations are caused by the generated shock wave for the 500-fs and 2-ps pulses and by the phase explosion for the 14.4-ps pulse.

In Fig. 7 the calculated ablation depth and the experimental data[25] are compared for gold ablated by a 150-fs laser pulse for the fluences up to 2 J/cm^2. The result calculated by Zavestovskaya et al.[25] is also plotted for comparison. Once more, the present model matches well with the experimental data. The two models deviate from each other when

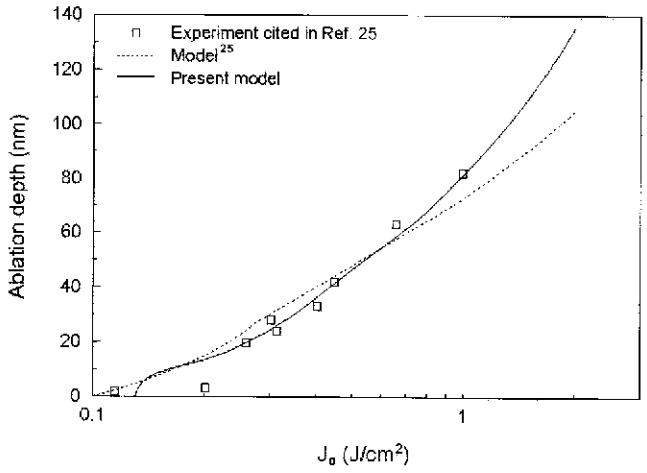

Fig. 7. Comparison of the simulated ablation depth with experimental data for gold heated by a 150-fs laser pulse ($\kappa = 0$).

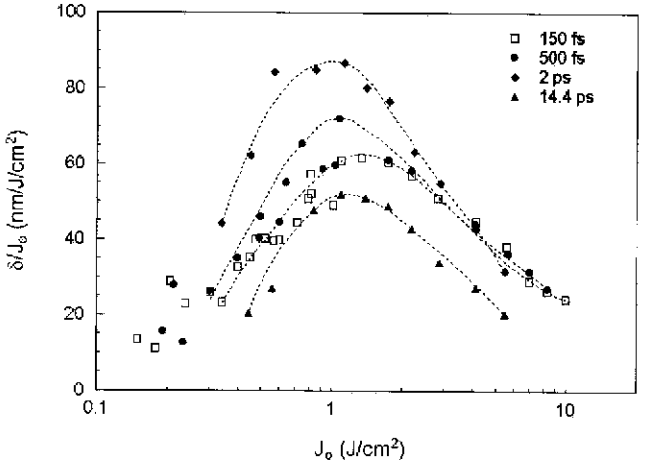

Fig. 8. Ablation rate versus laser fluence for copper heated by four ultrashort laser pulses.

the laser fluences are close to the ablation threshold and are higher than 0.8 J/cm^2. For this case, the ablation is nonthermal, caused by the generated shock wave.

The above simulations with different values of R and κ suggests that a comprehensive model for the entire process is needed, including the coupling of the laser beam with materials, ballistic motion and electron thermalization, thermomechanical response, superheating and phase transformation, formation and dynamics of the resulting plasmas and vapor, laser–plasmas/vapor interaction, and resolidification of the vapor and liquid. The material properties at extremely high heating rates and temperatures, such as the surface reflectivity, optical penetration depth, and thermophysical properties of electrons and the lattice (particularly in the liquid phase), also need to be characterized and quantified.

Laser ablation performance is one of the important factors that are of interest to the laser community. It is worth replotting the experimental data[18,25] in terms of the ablation rate

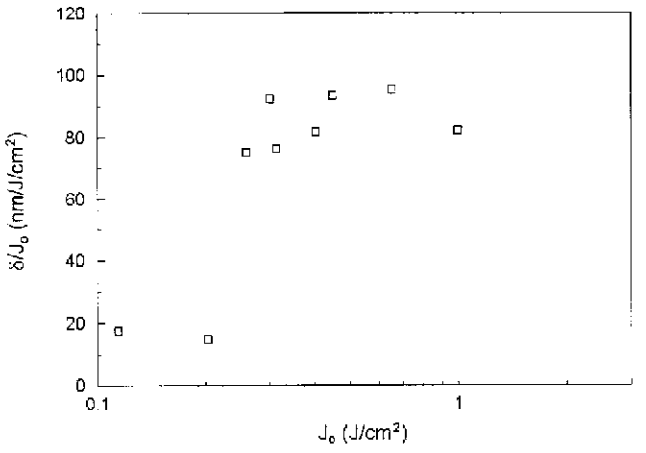

Fig. 9. Ablation rate versus laser fluence for gold heated by a 150-fs laser pulse.

(nm/J/cm^2) versus laser fluence. The results are shown in Fig. 8 for copper and Fig. 9 for gold. To better exhibit the trend of the scattered data in Fig. 8, dashed lines are drawn for the four fluences. For copper, as found in Fig. 8, the most efficient laser fluences are fairly close for all the pulses, about 1.1 J/cm^2. For the gold ablated by the 150-fs pulse (Fig. 9), the best ablation performance is found over a range of laser fluences from 0.3 to 0.8 J/cm^2.

5. Conclusions

A semiclassical two-temperature model is formulated to solve metals' thermal response caused by ultrashort laser illumination. With the first three moments of the Boltzmann transport equation, three equations that describe the conservation of number density, momentum, and energy are derived for the electron subsystem. The difference between the semiclassical and phenomenological 2T models is that the former take into account the effects of the electron drifting that is induced by the generated electric field and the electron kinetic pressure. In the simulation of the laser ablation, two competing mechanisms are considered: shock wave and phase explosion. The latter assumes that a laser ablation of a metal material occurs when the temperature of the superheated metastable liquid reaches the point near the thermodynamic equilibrium critical temperature, while the former assumes that the ablation occurs when the hot-electron kinetic pressure induced is higher than the characteristic pressure in a solid. Numerical analyses are performed for copper and gold films heated by ultrashort laser pulses. It is shown that the present approach correlates well with the experimental data over a wide range of laser fluences and pulse durations. It is also found that ultrafast laser ablation basically is caused by the generated shock wave for the pulses of a few picoseconds or shorter and by the thermally induced phase explosion for the longer laser pulses. Since the surface reflectivity and the parameter for the plasmas/vapor shielding of laser beams assumed in the present simulations vary with the pulse duration, a comprehensive model that includes the coupling of the laser beam with materials, thermomechanical response, superheating and phase transformation, formation and dynamics of the resulting plasmas and vapor, laser-plasmas/vapor interaction, and resolidification of the vapor and liquid is suggested.

References

[1]Abrikosov, A.A., *Fundamentals of the Theory of Metals*, Elsevier Science, Amsterdam (1988).

[2]Afanasiev, Y.V., B.N. Chichkov, N.N. Demchenko, V.A. Isakov, A.P. Kanavin, S.A. Uryupin, and I.N. Zavestovskaya, Proc. SPIE **3885**, 266 (2000).

[3]Anisimov, S.I., B.L. Kapeliovich, and T.L. Perel'man, Sov. Phys. JETP **39**, 375 (1974).

[4]Bulgakova, N.M., and I.M. Bulgakov, Appl. Surf. Sci. **197–198**, 41 (2002).

[5]Chen, J.K., and J.E. Beraun, Num. Heat Transfer A **40**, 1 (2001).

[6]Chen, J.K., and J.E. Beraun, J. Directed Energy **1**, 93 (2004).

[7]Chen, J.K., W.P. Latham, and J.E. Beraun, J. Laser Applic. **17**, 63 (2005).

[8]Cheng, C., and X. Xu, Appl. Phys. A **79**, 761 (2004).

[9]Gamaly, E.G., A.V. Rode, B. Luther-Davis, and V.T. Tikhonchuk, Phys. Plasmas **9**, 949 (2002).

[10]Ibrahim, W.M.G., H.E. Elsayed-Ali, C.E. Bonner, Jr., and M. Shinn, Int. J. Heat Mass Transfer **47**, 2261 (2004).

[11]Kelly, R., A. Miotello, A. Mele, A.G. Guidoni, J.W. Hastie, P.K. Schneck, and H. Okabe, Appl. Surf. Sci. **133**, 251 (1998).

[12]Kittle, C., *Introduction to Solid State Physics*, Wiley, New York (1967).

[13]Komashko, A.M., M.D. Feit, A.M. Rubenchik, M.D. Perry, and P.S. Banks, Appl. Phys A. **S69**, S95 (1999).

[14]Kruer, W. L., *The Physics of Laser Plasma Interactions*, Addison–Wesley, Redwood City, CA (1988).

[15]Leveugle, E., and L.V. Zhigilei, Appl. Phys. A **79**, 753 (2004).

[16]Madelung, O., *Introduction to Solid State Theory*, Springer, Berlin (1996).

[17]Momma, C., B.N. Chichkov, S. Nolte, F.V. Alvensleben, A. Tunnermann, H. Welling, and B. Wellegehausen, Optics Commu. **129**, 134 (1996).

[18]Nolte, S., C. Momma, H. Jacobs, A. Tunnermann, B.N. Chichkov, B. Wellegehausen, and H. Welling, J. Opt. Soc. Am. B **14**, 2716 (1997).

[19]Preuss, S., A. Demchuk, and M. Stuke, Appl. Phys. A **61**, 33 (1995).

[20]Schäfer, C., H.M. Urbassek, and L.V. Zhigilei, Phys. Rev. B **66**, 115404 (2002).

[21]Snowden, C.M., *Introduction to Semiconductor Device Modelling*, World Science, Singapore (1986).

[22]Vatsya, S.R., and K.S. Virk, J. Laser Applic. **15**, 273 (2003).

[23]Wellershoff, S.S., J. Hohlfeld, J. Gudde, and E. Matthias, Appl. Phys. A **69**[Suppl.], 99 (1999).

[24]Willis, D.A., and X. Xu, Int. J. Heat Mass Transfer **45**, 3911 (2002).

[25]Zavestovskaya, I.N., Y.V. Afanasiev, B.N. Chichkov, N.N. Demchenko, and V.A. Isakov, Proc. SPIE **3885**, 439 (2000).